Journal of Vacuum Science and Technology B

RESEARCH ARTICLE | MARCH 20 2026

Insights into the native structure of polyurea thickened lubricating grease via a multi-technique approach

Special Collection: Celebrating the Career of Prof. Jiro Matsuo and his Leadership in Gas Cluster Ion Beam Technologies and Secondary Ion Mass Spectrometry (SIMS)

Xiao Yuan L. Wang ; Christopher D. J. Parmenter ; Anna M. Kotowska ; Julie A. Watts; Davide S. A. De Focatiis ; Graham A. Rance ; David J. Scurr ; Derek J. Irvine

J. Vac. Sci. Technol. B 44, 024005 (2026)
https://doi.org/10.1116/6.0005074

JVST B
Journal of Vacuum Science & Technology B

ARTICLE

pubs.aip.org/avs/jvb

Insights into the native structure of polyurea thickened lubricating grease via a multi-technique approach

Cite as: J. Vac. Sci. Technol. B 44, 024005 (2026); doi: 10.1116/6.0005074
Submitted: 16 October 2025 · Accepted: 18 February 2026 ·
Published Online: 20 March 2026

Xiao Yuan L. Wang,[1] Christopher D. J. Parmenter,[2,3] Anna M. Kotowska,[2,3] Julie A. Watts,[2] Davide S. A. De Focatiis,[4] Graham A. Rance,[2,5,a)] David J. Scurr,[3,a)] and Derek J. Irvine[1,6,a)]

AFFILIATIONS

[1]Department of Chemical and Environmental Engineering, University of Nottingham, Nottingham NG7 2RD, United Kingdom
[2]Nanoscale and Microscale Research Centre (nmRC), University of Nottingham, Nottingham NG7 2RD, United Kingdom
[3]School of Pharmacy, University of Nottingham, Nottingham NG7 2RD, United Kingdom
[4]Composites Research Group, University of Nottingham, Nottingham NG7 2RD, United Kingdom
[5]School of Chemistry, University of Nottingham, Nottingham NG7 2RD, United Kingdom
[6]Centre for Additive Manufacturing, University of Nottingham, Nottingham NG7 2RD, United Kingdom

Note: This paper is part of the Special Topic Collection Honoring Dr. Jiro Matsuo's 65th Birthday and his Leadership in Ion Beam Analysis and SIMS.

a)Authors to whom correspondence should be addressed: Graham.Rance@nottingham.ac.uk; David.Scurr@nottingham.ac.uk; and Derek.Irvine@nottingham.ac.uk

ABSTRACT

Polyurea greases play an important role in the operation of electric vehicles, and it is understood that their performance is principally determined by their microstructure. Consequently, developing a complete understanding of the structural characteristics of polyurea greases is crucial for the future engineering of new greases. One of the most widely used techniques for urea grease analysis is scanning electron microscopy (SEM). However, this requires the removal of the base oil component prior to analysis and hence does not give a true picture of the grease microstructure. Alternative techniques, including polarized optical microscopy (POM) and cryogenic SEM (cryo-SEM), do not require base oil removal, but fail to provide the chemical information required to definitively discriminate between the base oil and thickener components. In this study, we pioneered the use of a novel combination of native- and near-native-state chemical imaging techniques, namely, confocal Raman microscopy (CRM) and cryogenic secondary ion mass spectrometry (cryo-SIMS), to characterize a commercial polyurea grease sample. It was possible to detect peaks diagnostic of polyurea in CRM, and the urea species known to be present in the grease in cryo-SIMS. In the chemical imaging analyses, distinct particles of polyurea (~250–280 μm^2) were observed, broadly consistent with observations from POM of the same material. Such findings increase confidence that POM, the most straightforward native-state technique applicable for polyurea grease analysis, can be reliably used to understand the key structure-performance relationships that will ultimately guide the development of future polyurea greases.

I. INTRODUCTION

Polyurea thickened lubricating greases (polyurea greases) display desirable temperature properties and inherent resistance to oxidation[1–4] and are therefore gaining increasing attention as lubricants in electric vehicle motors.[5] Unlike liquid lubricants, consisting of a base oil (mineral or synthetic oil) and additives only, polyurea greases are semisolid lubricants containing a thickener (typically a polyurea compound, ~5–25 wt. %) in addition to the base oil and additives.[6,7] Thickeners are examples of low molecular weight gelators,[8] which typically comprise small molecules that

can self-assemble through noncovalent interactions (e.g., hydrogen bonds, van der Waals forces, π-π interactions, and electrostatic interactions) to form a network that immobilizes the liquid base oil.[8–14]

The performance (i.e., rheology and oil release mechanism) of polyurea grease is largely dependent on the microstructure formed by the thickener.[11,12,15] Characterizing and understanding the physicochemical structure of polyurea grease is, therefore, crucial for the development of new greases with improved lubricating performance.[16] Toward this end, the microstructure of polyurea greases has been previously studied by separating the base oil from the thickener network through washing with a suitable solvent, thus enabling analysis of the thickener using electron microscopy.[16] For example, Cyriac *et al.*[17] used scanning electron microscopy (SEM) and reported polyurea grease possessing thickeners in the form of platelets with an average length of ∼1.5 μm and an average width of ∼1.2 μm. Ren *et al.*[18] synthesized polyurea greases containing different ureido amounts and observed their morphologies with SEM. They reported that, of the materials that were included in their study, the tetraurea structures exhibited a packed granular structure and provided the most improved physicochemical properties. Wang *et al.*[12] synthesized polyurea grease with poly(α-olefin) base oil and observed the thickener morphology via SEM. The grease thickener formed fibers that interweaved to generate a three-dimensional porous network, exhibiting low oil separation (0.3%) and a high dropping point (280 °C). Fan *et al.*[7] synthesized polyurea grease and utilized transmission electron microscopy (TEM) to analyze the grease structure. The grease displayed excellent colloid stability, which was attributed to its compact 3D network structure linked together due to interactions between the thickener molecules.

However, it is understood that the act of washing the base oil out results in contraction of the thickener-oil network and, therefore, a collapsed grease structure that is not necessarily an accurate representation of the actual thickener structure present in the oil.[12,16,19,20] Polarized optical microscopy (POM) is one technique that does not require base oil removal and is comparatively quick, cheap, and easy to conduct. Wang *et al.*[12,21] and Wu *et al.*[22] utilized POM for native-state analysis of polyurea greases, in combination with conventional SEM, noting key differences in the thickener structures observed using the two techniques. This was attributed to the removal of the base oil for the SEM analysis, disrupting the original structure of the thickener.

Cryogenic electron microscopy is a further technique that does not require base oil removal and has been explored by Thorseth *et al.*[16] for the characterization of polyurea grease, evidencing agglomerates of polyurea. The authors noted that, by combining cryo-microtomy and TEM imaging, a microstructure with complex morphology, including entangled fibrous clusters, aligned chains and sheets, was observed.[11,16] In general, microscopy techniques that do not require base oil removal provide a more accurate representation of the thickener structure. However, in the absence of staining, it can be challenging to differentiate between the thickener and base oil.[16,23] To overcome this, chemical imaging can be used. For example, cryogenic scanning electron microscopy (cryo-SEM) can be combined with spatially-correlated energy dispersive x-ray (EDX) analysis; however, this provides limited information on chemical composition, yielding at most the identity and distribution of elements.[24]

On the other hand, confocal Raman microscopy (CRM) and secondary ion mass spectrometry (SIMS) are complementary label-free chemical imaging techniques.[25] CRM provides detailed insights into molecular vibrations and thus chemical bonding.[26] The technique requires minimal sample preparation and operates nondestructively, hence permitting analysis of samples in their native state.[26] Furthermore, it offers a limiting lateral resolution of ∼200–300 nm (depending on instrument configuration) as defined by the optical diffraction limit.[27] The chemical identification capability of Raman spectroscopy has been utilized in previous studies on lubricating grease for various applications. For example, to monitor the change in molecular structure of lithium stearate-thickened grease modified with montmorillonite after tribological tests[28] and to understand the mechanism of decomposition[29] and the kinetics of tribofilm formation[30] of the molybdenum dialkyl dithiocarbamate friction modifier.

SIMS offers detection of both single elements and molecules and can produce three-dimensional chemical maps that combine molecular information with nanometer depth resolution, i.e., <10 nm.[31] Time-of-flight secondary ion mass spectrometry (ToF-SIMS), used in combination with a liquid metal ion gun (LMIG) primary ion beam, offers fast data acquisition and imaging with high lateral resolution (<50 nm).[31–33] However, LMIG beams are highly energetic and are known to cause considerable fragmentation of the sample of interest, resulting in a loss of molecular information of the detected ions.[34] The OrbiSIMS, developed in 2017, combines a time-of-flight and Orbitrap analyzer and utilizes both an LMIG and gas cluster ion beam (GCIB).[35] The GCIB is comprised of large clusters of particles; as a result, the energy per atom is significantly reduced compared to a monatomic ion beam and their collision energy is concentrated on the surface.[36–38] Consequently, they can generate mass spectra with less fragmentation and display high depth resolution.[36,37] Combined with the high mass resolving power (>240 000 at m/z 200) and mass accuracy (<1 ppm) of an Orbitrap,[34,35,39,40] this allows for 3D chemical imaging and visualization of a sample's internal structure.[36]

To characterize samples with volatile phases, such as polyurea grease, in their near-native state via SIMS, analysis at cryogenic temperatures is necessary due to the inherent incompatibility of such samples with the ultrahigh vacuum of an SIMS instrument. Examples of studies that have used cryogenic secondary ion mass spectrometry (cryo-SIMS) for structural characterization of challenging samples in their near-native state include those by Taylor *et al.*[41] (hydrogel films), Zhang *et al.*[39] (biofilms), Newell *et al.*[42] (tissue), Starr *et al.*[43] (skin), and Akbari *et al.*[44] (biofilms).

To the best of our knowledge, there have been no previous studies employing cryo-SIMS and CRM for the imaging of polyurea grease. In this study, we imaged a commercial polyurea grease using a combination of POM, CRM, cryo-SEM combined with EDX spectroscopy, and cryo-SIMS. Through careful correlation of polyurea particle sizes obtained using this holistic approach, we conclude that POM analysis alone—an approach that is easy to perform, tolerant of ambient conditions thus preserving the native state and providing robust and meaningful statistics—can be used with confidence to probe the microstructure of polyurea grease.

II. EXPERIMENT

A. Materials

A sample of the commercial base polyurea grease and fresh base oils used in the manufacture of this sample was provided by an external sponsor. The full composition of this grease sample (provided by the external sponsor) is shown in Table S1 in the supplementary material. The reagents and manufacturing process used to synthesize this grease sample and the reaction mechanism understood to drive its formation (provided by the external sponsor) are illustrated in Figs. S1 and S2 in the supplementary material, respectively.

The polyurea thickener was separated and isolated from the parent grease sample via a Soxhlet extraction. Commercial base polyurea grease was placed in a preweighed cellulose thimble (Cytiva Whatman, 25 × 90 mm). The thimble was filled with 24.2 g of grease and then placed in a Soxhlet extractor. This was then fitted with a 250 ml round-bottomed flask half-filled with hexane (99%, Fisher) and cooled using a water-flow condenser. The apparatus was left extracting at 100–105 °C (temperature range selected due to variations in laboratory temperatures throughout the course of the experiment) for 48 h to allow the hexane solvent to extract the base oils from the surface of the particles. Upon completion of the extraction, the thimble was placed in a room temperature vacuum oven for at least 12 h to dry under vacuum. Confirmation that a 48 h procedure was sufficient to lead to the removal of the base oil from the particle surfaces was obtained by recording the mass of vacuum-dried sample remaining in the thimble and comparing the reduction in mass with the composition of the grease (Table SI in the supplementary material). 4.58 g of commercial grease sample remained, representing a reduction in mass of 81.1%, which is approximately equal to the base oil composition of the grease sample (80.3 wt. %). All investigations detailed in this study that included analysis of extracted polyurea thickener utilized the vacuum-dried thickener obtained from this extraction.

B. Optical microscopy

Optical microscopy images (nonpolarized and polarized) were obtained using an Olympus BX51 light microscope. To prepare the sample for analysis, a spatula was first dipped into the grease and used to smear a small amount across the surface of a glass microscope slide. A coverslip was then pressed onto the grease smear to ensure it was as flat as possible. Images were collected in transmission brightfield mode, using a 10× (0.3 N_A), 20× (0.5 N_A), or 50× (0.5 N_A) metallurgic objective.

C. CRM

Confocal Raman microscopy analysis was conducted using a HORIBA XploRA INV Raman microscope. Before data collection, the instrument was calibrated using the Si (100) peak at 520.7 cm^{-1}. Spectra were acquired using a 785 nm laser (Innovative Photonic Solutions) at 100% power, a 100× (0.8 N_A) objective, a 100 μm entrance slit, a 100 μm confocal pinhole, and a 600 lines mm^{-1} diffraction grating. During measurement optimization, the stability of all components of the fully formulated grease to the maximum laser power was verified, as is standard practice. The spectral resolution in this configuration is better than 3.1 cm^{-1}. The lateral (xy) spatial resolution (theoretically 599 nm, using $0.61\lambda/N_A$) was experimentally measured using 100 nm-wide gold stripes on Si as 1149 nm. The axial (z) spatial resolution [theoretically ~4.9 μm, using $4\lambda/(N_A)^2$] was approximated by axial mapping of Si as 4.4 μm.

Single-point Raman spectra of the fresh base oils (API category Group V ester and high viscosity polyalphaolefin, see Table S1 in the supplementary material) and polyurea thickener (extracted from the commercial base polyurea grease via Soxhlet extraction as detailed in Sec. II A) were collected to enable referencing. Spectra were acquired over the range 200–2000 cm^{-1} with 15–60 s integration time and 4 accumulations to remove spikes from cosmic rays and improve the signal-to-noise ratio. The spectrum of the extracted polyurea thickener was obtained after 5 min of photobleaching.

For multiple-point Raman imaging analysis, spectra were acquired over the range 200–2000 cm^{-1}, with 5 s integration time and 2 accumulations in either: (i) 1 μm steps from within a 100 × 100 μm area (10 201 spectra in total) or (ii) 2 μm steps from within a 300 × 300 μm area (22 801 spectra in total). In either case, the sample was prepared by sandwiching a small quantity of the grease between two quartz microscope cover slips. False color images showing the distribution of polyurea particles within the base oil matrix were generated using univariate analysis within LABSPEC 6.7 software by plotting the intensity (as peak height) of a diagnostic Raman peak of the polyurea thickener (either ~1133 cm^{-1}, within the range 1120–1145 cm^{-1}, or ~1062 cm^{-1}, within the range 1050–1070 cm^{-1}) as a function of spatial location. Images were also generated by application of multivariate curve resolution (MCR). In this case, two loadings were extracted, with the corresponding images generated by plotting the respective scores for each MCR loading (normalized to a total of 100% across the two loadings) at each location.

D. Cryo-SEM and EDX

Cryo-SEM and EDX analyses were conducted using a Zeiss Crossbeam 550 (Carl Zeiss, Germany). The grease was smeared onto a cryo-SEM rivet, which was then plunged into slushy nitrogen and allowed to freeze. The frozen sample was transferred to a cryo-preparation chamber (Quorum 3010, Quorum Technologies Ltd, Loughton, UK), which had been cooled to −150 °C. Here, it was fractured with a cooled blade, sublimed at −90 °C for 3 min and sputter coated with platinum at 10 mA for 60 s. The fractured sample was then transferred to the main chamber for SEM and EDX analysis. The accelerating voltage of the SEM was operated at 2 or 5 kV for imaging. EDX was performed using an Oxford Instruments UltimMax 170 detector, the SEM used an accelerating voltage of 5 kV, and data were analyzed using AZTEC software (version 6.1).

E. Cryo-ToF-SIMS and cryo-OrbiSIMS

ToF-SIMS and OrbiSIMS were conducted using a Hybrid SIMS instrument (IONTOF GmbH) under cryogenic conditions (< −160 °C). The analysis was conducted based on the protocol detailed by Zhang *et al.*[39]

Prior to SIMS analysis, the commercial base polyurea grease and the pure base oils used in the manufacture of this sample

(Table S1 in the supplementary material) were plunge frozen and then transferred to the main chamber of the SIMS instrument for analysis using a shuttle chamber Leica EM VCT500 (Leica, Germany). The temperature at transfer is −150 °C, and the SIMS instrument airlock and main chamber were precooled. The detailed sample preparation and transfer procedure is described in *Procedure S1* of the supplementary material, and a flow diagram of the sample preparation is illustrated in Fig. S3 in the supplementary material.

A region where the sample was flattest was identified. For ToF-SIMS analysis of all the samples, a 30 keV Bi_3^+ LMIG with a pulsed target current of ∼0.03 pA and a spot size of <120 nm was used as the primary ion beam and a 20 keV Argon (Ar_{2027}^+) GCIB, which has a beam diameter of 110 μm and a current of 3.6 nA was used as the sputter beam with a 700 × 700 μm crater size. Data were collected over a 500 × 500 μm area using random raster mode, with a 256 × 256 pixel raster size. Noninterlaced depth profiling was employed, whereby the sputter and analysis ion beams operate at alternating intervals with 15 s of sputtering per 1 analysis frame and a 0.5 s pause between the sputtering and analysis. A cycle time of 200 μs was used, and the analysis was performed at < −160 °C. The data were collected using delayed extraction for optimal mass and lateral resolution as well as mitigating topography effects. A low energy electron floodgun and argon gas flooding were in operation to aid charge compensation, and the pressure in the main chamber was maintained at 9.0×10^{-7} mbar. The data were collected in negative polarity.

For OrbiSIMS analysis of all the samples, a 20 keV Argon (Ar_{3079}^+) GCIB with a spot size of 20 μm, a beam diameter of 20 μm, and a primary beam current of 245 pA was used with a 384.6 × 384.6 μm crater size. Data were collected over a 300 × 300 μm area. A mass range of *m/z* 75–1125, a mass resolution of 240 000, and a temperature of <−160 °C were used for the analysis. A low energy electron floodgun and argon gas flooding were in operation to aid charge compensation, and the pressure in the main chamber was maintained at 9.0×10^{-7} mbar. Orbitrap QExactive HF was used as the analyzer, and the collisional cooling was set to low pressure (3.0×10^{-7} mbar). The data were collected in negative polarity. Data analysis was performed using SURFACELAB 7.3 software, and ToF-SIMS data were calibrated using $O_4H_7^-$, $O_5H_9^-$, $O_6H_{11}^-$, $O_7H_{13}^-$, $O_8H_{15}^-$, and $O_9H_{17}^-$, ions.

F. Image analysis

Images of the commercial base polyurea grease obtained from all techniques were processed in ImageJ (Version 1.54i). The size and shape of all particle structures in each image field of view was obtained following a similar protocol detailed by Zhao *et al.*[45] The unit of pixels was converted to micrometers according to the scale bar. The image threshold was set using the Auto-threshold function, and the "Default" thresholding algorithm was used for all analyses detailed in this study. Holes in particles were filled automatically using the "Binary" function. The "Analyze Particles" function was then used to obtain the area (range: 40–infinity μm^2, selected to exclude objects indistinguishable as particles) and circularity (range: 0–1) of all particles within the threshold. The "Exclude on edges" option was selected to avoid measuring partial objects.

III. RESULTS AND DISCUSSION

A. Understanding the morphology of lubricating grease with optical microscopy

POM enables analysis in the native state, is quick, cheap, and easy to conduct and so represents the ideal technique for structural investigation of lubricating grease. Figure 1 shows optical micrographs of the commercial base polyurea grease collected in one area of interest of the grease sample smeared on the glass slide.

The area and circularity histograms of the particles identified in the polarized optical micrographs of Fig. 1 are shown in Fig. 2.

The images obtained from optical microscopy were largely featureless. On the other hand, POM revealed two distinct phases, increasing confidence that this technique can discriminate between the polyurea thickener and base oil phases. To help confirm the identity of the bright spots in Fig. 1, polarized optical microscope images of the polyurea thickener extracted from the commercial sample via Soxhlet and of the pure base oils were collected (Fig. S4 in the supplementary material). The extracted polyurea thickener appears bright when viewed under a polarizer, whereas the base oils do not, evidencing that the bright spots in Fig. 1 are the polyurea thickener in the form of distinct particles. Polymeric materials are typically anisotropic and upon interaction with polarized light generate interference effects that result in differences in brightness and color of the image (birefringence).[46] Moreover, the extracted polyurea thickener particles are significantly larger than the particles in the intact grease formulation (Fig. 2 and Fig. S5 in the supplementary material). Removal of the base oil phase is known to collapse the three-dimensional structure of grease and result in the formation of agglomerates. This collapse is likely due to the hydrogen bonding network that forms in polyureas.[16]

Repeat optical microscopy images were collected from a second region of interest from the same sample with the images shown in Fig. S6 in the supplementary material and the corresponding particle area and circularity histograms in Fig. S7 in the supplementary material. As shown in Fig. 2 and Fig. S7 in the supplementary material, the particles observed in the polarized optical micrographs of Fig. 1 and Fig. S6 in the supplementary material show an average area of 160–220 μm^2. It is worth noting, however, that the area distribution exhibits a positive skew and particles of 1000–4000 μm^2 (Fig. 2) were detected. It is also noted that on observation the particles display a range of shapes; this becomes particularly apparent at higher (50×) magnification. This is further supported by the circularity histograms where, in general, the average circularity is <0.500. The mean circularity at 50× magnification is notably smaller than that recorded at 10× and 20× magnification. As the particles observed are significantly larger than the limiting optical resolution, this is likely due to the reduced number of particles inherently available to be sampled at higher magnification.

In summary, it has been further justified that analyzing extracted thickeners does not give a true representation of the structure of polyurea grease due to the formation of agglomerates. POM would be an ideal technique for the native-state structural characterization of lubricating grease. However, due to a lack of chemical information the technique offers, definitive identification of the phases observed can only be speculated. As such, more detailed chemical analysis is needed to further confirm the suitability of

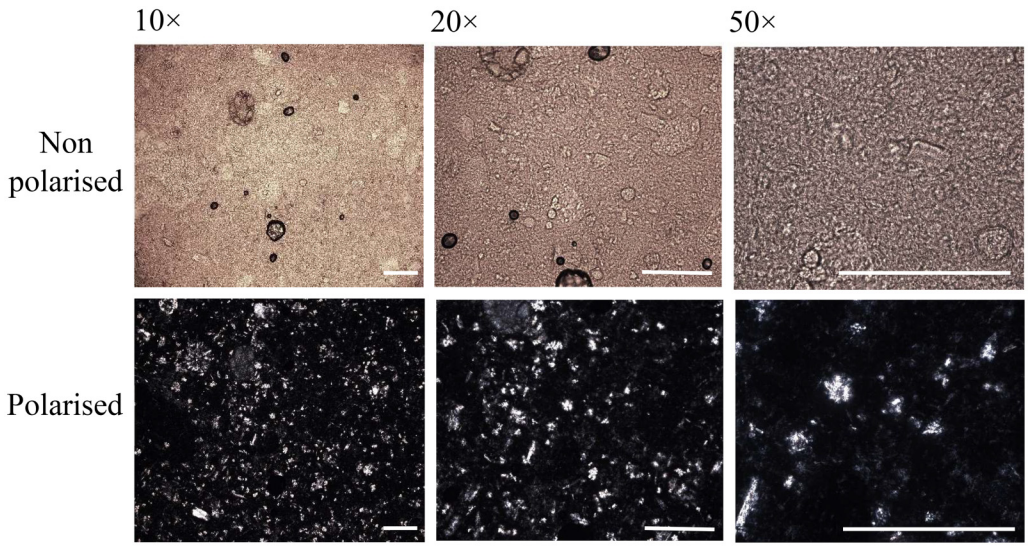

FIG. 1. Transmission brightfield optical microscopy images of the commercial base polyurea grease, collected with a 10×, 20×, and 50× objective. All images were collected from the same region of interest. Scale bars = 200 μm.

optical microscopy as a tool for structural characterization of lubricating grease.

B. Chemical identification with CRM

Like optical microscopy, CRM enables native-state analysis of molecular materials with no significant sample preparation typically required. Moreover, CRM provides molecular fingerprint chemical analysis and when combined with automated sample movement and appropriate data analysis strategies can be used to generate false color images describing chemical composition with a spatial resolution limited by optical diffraction. In this study, CRM was utilized to confirm the identity of the different phases observed in the previously discussed optical microscopy analysis of the commercial base polyurea grease (Fig. 3).

To identify a Raman peak diagnostic of the polyurea thickener phase, critical for subsequent image generation, point Raman spectra of the grease components, i.e., the two pure base oils, plus the polyurea thickener extracted via Soxhlet extraction, were collected [Fig. 3(a)]. Full assignment of peaks in the Raman spectra of the specific molecular species explored here has not been reported previously and is beyond the scope of our investigation; however, Raman spectroscopy analysis of related polyalpha olefin oils (cf. high viscosity polyalpha olefin)[47] and N-alkylated ureas (cf. extracted polyurea)[48] has been performed, with the spectra observed here consistent with these prior studies. Of note, the narrow peak at 1133 cm^{-1} in the Raman spectrum of the extracted polyurea, likely representing degenerate ν(CN), ν(CC), and δ(CH_2) vibrational modes,[48] appears to be indicative of the thickener phase. Subsequent preliminary Raman imaging from a relatively small area (100 × 100 μm), where the intensity of the 1133 cm^{-1} peak was plotted as a function of spatial location (Fig. S8 in the supplementary material), evidences particle-like structures. An analogous image was constructed using the intensity of the 1062 cm^{-1} peak (Fig. S8 in the supplementary material), assigned as degenerate ν(CC) and ν(CN) vibrational modes,[48] though the image contrast was notably lower.

On inspection, it was noted that the shape of the structures in Fig. S8 in the supplementary material was close to those observed in the POM analysis (Fig. 1 and Fig. S6 in the supplementary material). Further Raman imaging and analysis from a larger area (300 × 300 μm) [Fig. 3(b) and Fig. S9 in the supplementary material] enabled quantification of the distribution of particle area and circularity (Fig. 4).

Here, it can be concluded more confidently that the size and shape of the particle-like structures observed in CRM [Fig. 3(b)] are comparable to those identified in POM (Fig. 2 and Fig. S7 in the supplementary material). This provides further evidence that the bright spots observed in the POM analysis (Fig. 1 and Fig. S6 in the supplementary material) are indeed particles of polyurea. To negate any potential issues with spectral overlap and improve the clarity of the images, multivariate curve resolution was applied to the two datasets (Figs. S10 and S11 in the supplementary material). In both cases, two loadings were extracted, one predominantly consistent with the base oil (MCR A) and the other with the polyurea thickener (MCR B). The images generated by plotting the scores associated with MCR B strongly match the images obtained using the respective univariate analysis approaches described above. Thus, CRM provides direct chemical evidence, based on the molecular fingerprint, for the existence of the polyurea thickener as particle-like features within a base oil matrix. However, it is important to note that the Raman scattering cross sections of all components explored here are relatively low and consequently Raman imaging is slow (the maps shown in Fig. S8 in the supplementary material and

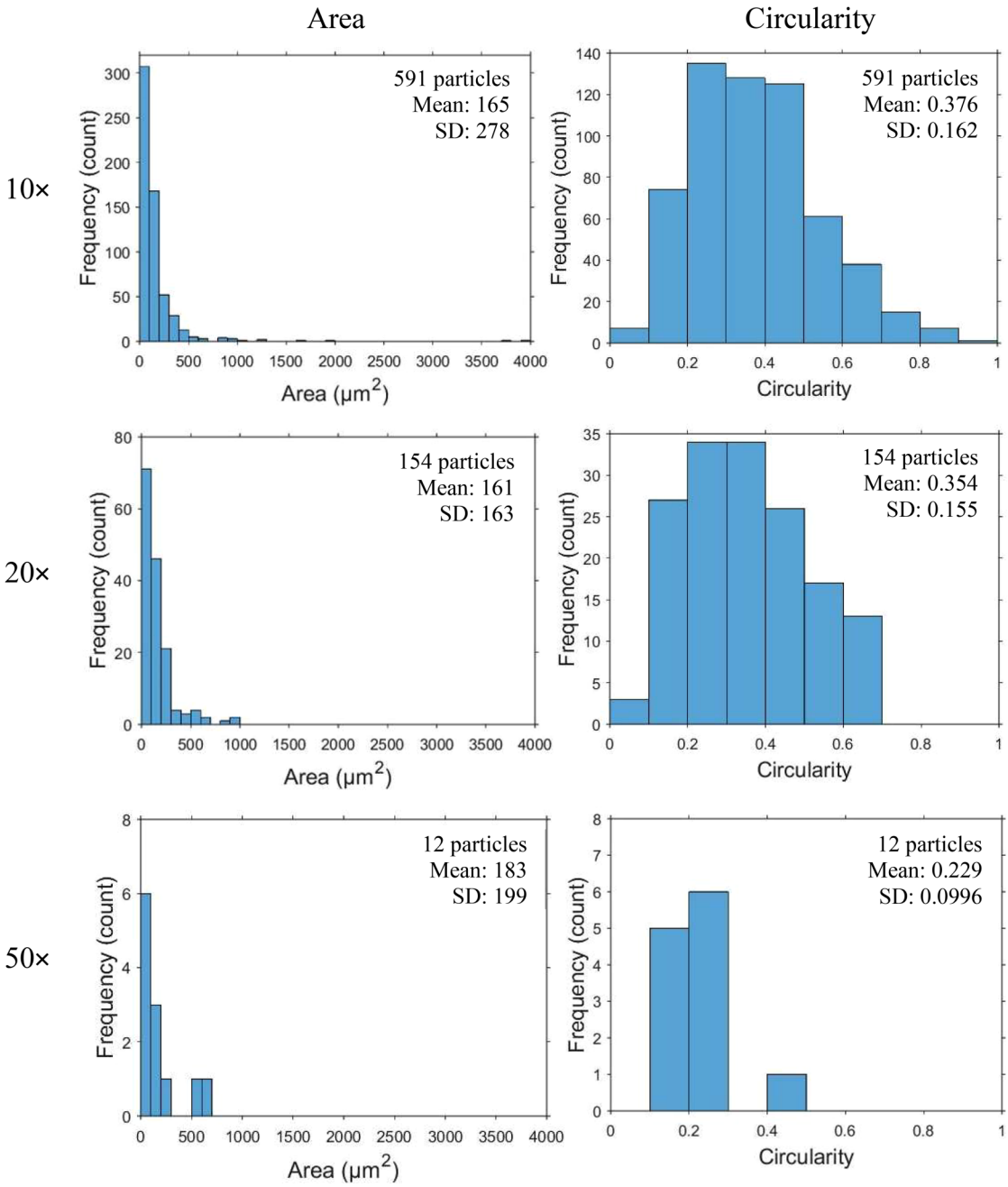

FIG. 2. Particle area (left column) and circularity (right column) determined from the polarized optical microscope images displayed in Fig. 1. The number of particles sampled, mean, and standard deviation (SD) are also shown.

Fig. 3 took ~27 and ~66 h to obtain, respectively). In addition, the depth resolution [approximated as $4\lambda/(N_A)^2$, where λ is the wavelength of the laser and N_A is the numerical aperture of the objective lens][49] is typically on the order of micrometers and incredibly challenging to determine experimentally with accuracy, and therefore any spectrum obtained from a given polyurea particle may contain potential contribution from the out-of-focus base oil immediately above or beneath. Complementary analytical

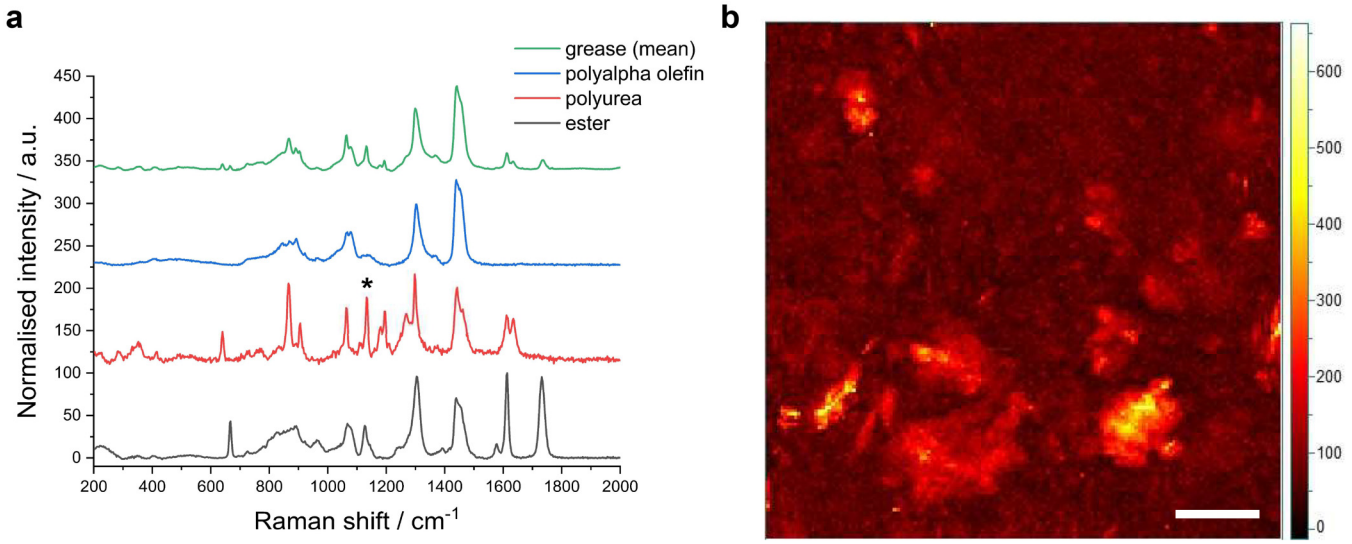

FIG. 3. CRM analysis of the commercial base polyurea grease. (a) Single-point Raman spectra of the individual components of the grease formulation, in addition to the mean spectrum extracted from the mapping analysis of the fully formulated grease. Spectra have been baseline-corrected, normalized to the intensity of the spectral maximum and offset on the y-axis to enable ease of visual comparison. (b) A false-color Raman image (obtained from a 300 × 300 μm area in 2 μm steps) showing the distribution of the polyurea thickener. The color scale shows the intensity (counts) of a peak in the Raman spectrum uniquely diagnostic of polyurea [at ~1133 cm^{-1}, annotated with an asterisk in (a)]. Scale bar = 50 μm.

approaches, ideally those that are both faster and more surface-sensitive, but provide analogous chemical information, would therefore be desirable.

C. Chemical identification with cryo-SEM EDX

Cryo-SEM is a near-native-state imaging technique that can be used with spatially-correlated EDX analysis to provide combined morphological and elemental information from a given sample. Although EDX analysis is limited to the identification of elements,[24] it is known that the polyurea thickener phase contains nitrogen, whereas the base oil phase does not (Table S1 in the supplementary material). Hence, the presence of nitrogen can, in principle, be used to differentiate between the suspected thickener and base oils phases. Cryo-SEM images and EDX maps of the commercial base polyurea grease are shown in Fig. 5.

Whilst some regions of the grease were featureless [Fig. S12(a) in the supplementary material], particle-like features, pseudospherical in morphology, were identified in the cryo-SEM images of the commercial polyurea grease sample [Fig. 5(a) and Figs. S12(b)–S12(h) in

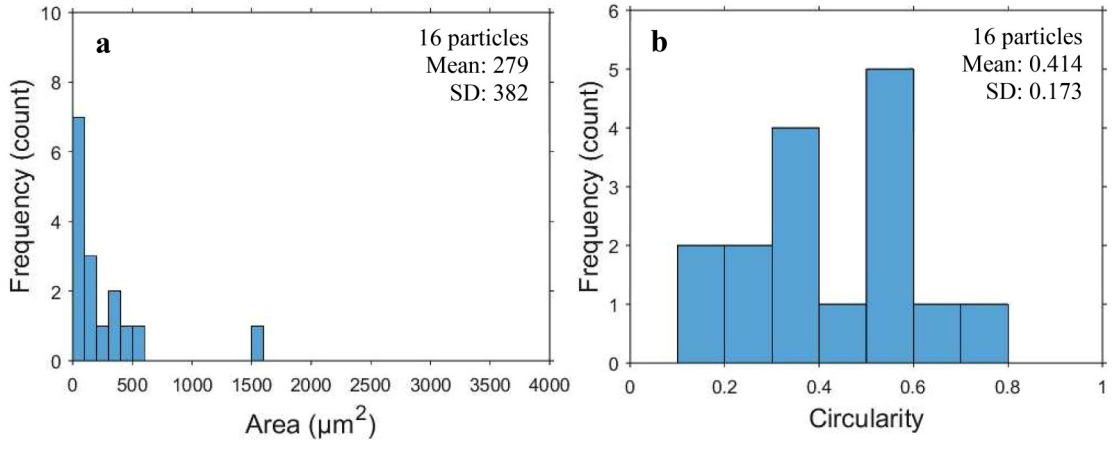

FIG. 4. Particle area (a) and circularity (b) histograms summarizing determined from the Raman image shown in Fig. 3(b).

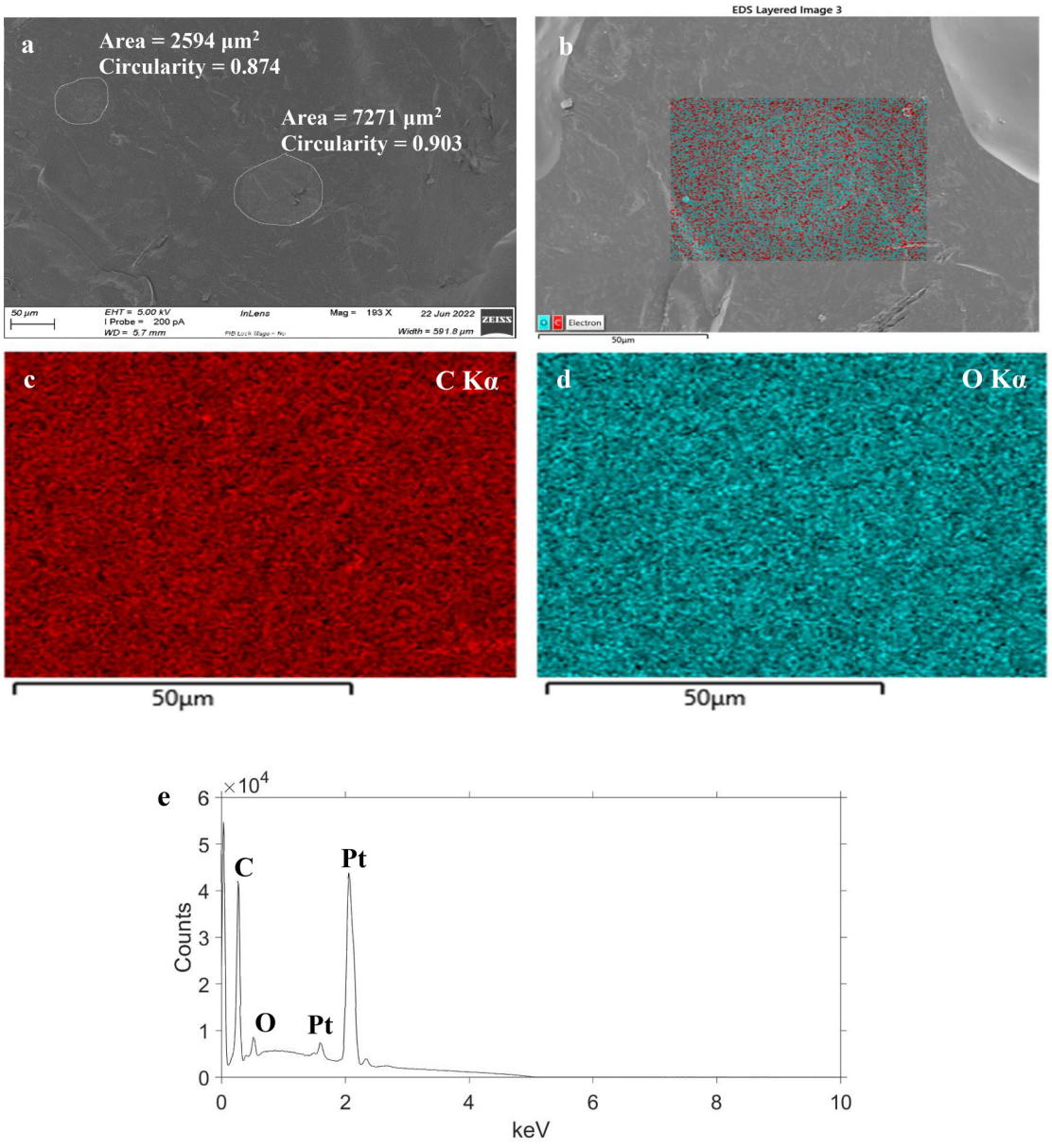

FIG. 5. Cryo-SEM and EDX analysis of the commercial base polyurea grease. (a) Possible particles of polyurea thickener. White dashed lines guide your eye to the location of the particles. Scale bar = 50 μm. (b) A possible particle of polyurea thickener selected for EDX mapping, showing the overlaid C and O Kα x-ray emissions. EDX map showing the (c) C and (d) O Kα x-ray emission. Scale bars = 50 μm. (e) The resultant mean EDX spectrum. The Pt signal originates from the sputter coating.

the supplementary material]. It is noted that some of these features are significantly larger and more circular than many of the particles identified in the POM analysis (Figs. 1 and 2) and less abundantly observed. Cryogenic sample preparation can introduce artifacts via (a) ice crystal formation and (b) contamination. When freezing samples with slushy nitrogen, the rate of cooling of the samples is typically not rapid enough to prevent ice crystal formation, and the latter subsequently can damage sample structures;[50] however, this applies to samples that have a high water content, as it is the water that crystallizes to ice. In the case of this oil and polyurea mixture, which has very little (if any) water, we do not believe this to have been an issue. Additionally, surface contamination by condensed volatiles is another potential issue when imaging cryo-fractured specimens;[51] yet, this is also typically associated with hydrated samples.

Also, the sample was sublimed post fracture to remove any surface frost that may have been formed during freezing. No evidence of frost contamination was observed during imaging.

To probe the identity of the features shown in Fig. 5(a) and Figs. S12(d)–S12(h) in the supplementary material, one of these particles was selected for EDX analysis [Fig. 5(b)]. The mapping [Figs. 5(c) and 5(d)] indicated that both carbon and oxygen were present within the entire imaged area, i.e., over both the selected particle and the surrounding matrix. Specifically, 85.9 wt. % carbon and 14.1 wt. % oxygen levels were observed. This was expected as both the polyurea thickener and base oil components contain carbon and oxygen (Table S1 in the supplementary material). Importantly, no significant nitrogen was detected [Fig. 5(e)]; however, it is known that nitrogen can be challenging to detect using EDX as the nitrogen Kα x-ray emission (0.392 eV) overlaps with that of carbon (0.277 eV), making it difficult to deconvolute the nitrogen signal from carbon.[52] Thus, while cryo-SEM provides further evidence that the commercial base polyurea grease exists in

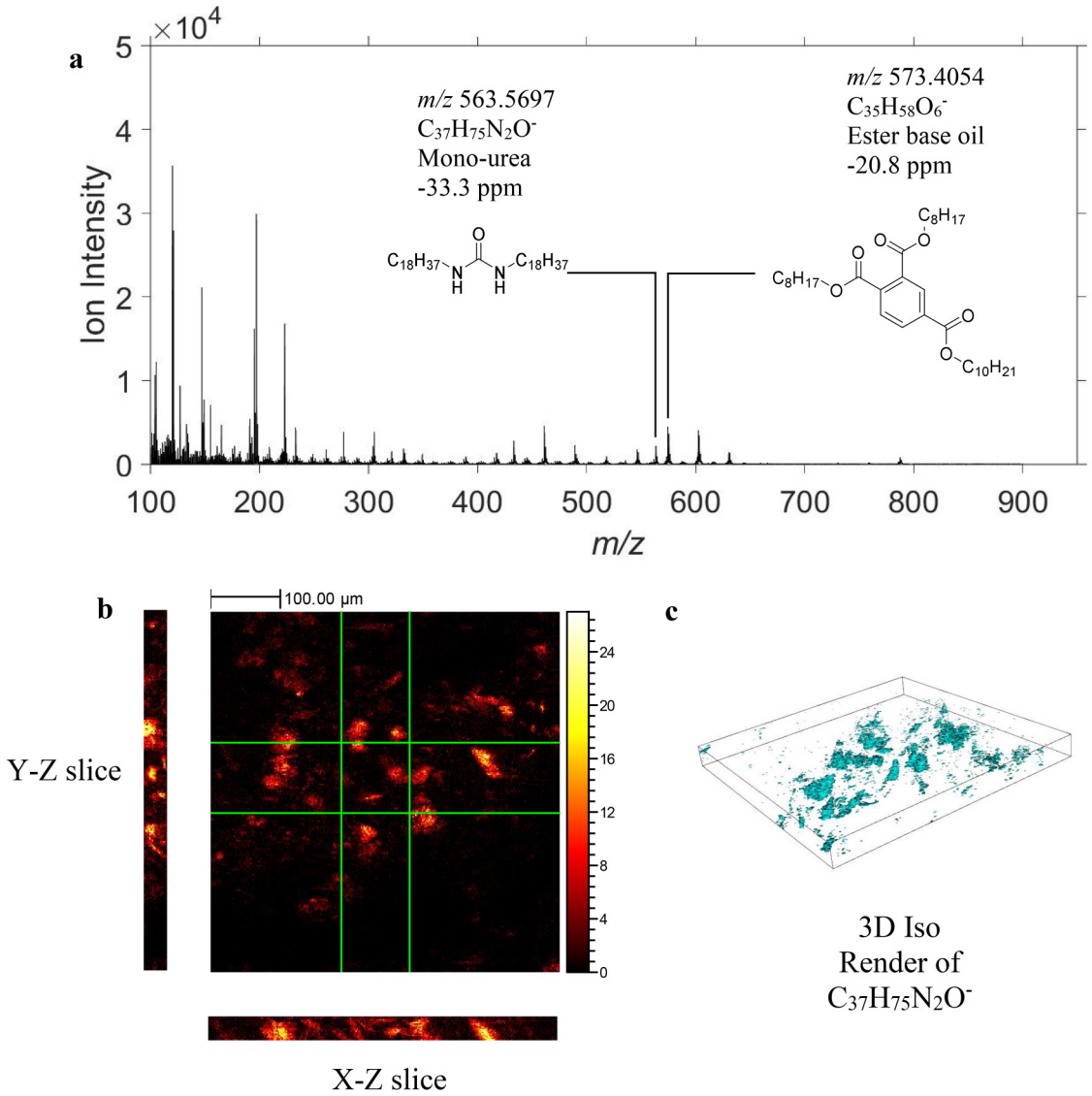

FIG. 6. Negative polarity ToF-SIMS data of plunge frozen commercial polyurea grease. (a) ToF-SIMS spectrum, showing the mono-urea molecular and ester base oil ions. (b) Secondary ion image of the mono-urea X-Y view of 3D dataset where the green lines indicate the position of the Y-Z and X-Z slices shown. The color scale shows the secondary ion intensity and scale bar = 100 μm. (c) 3D isometric render of the mono-urea ion image shown in Fig. 6(b).

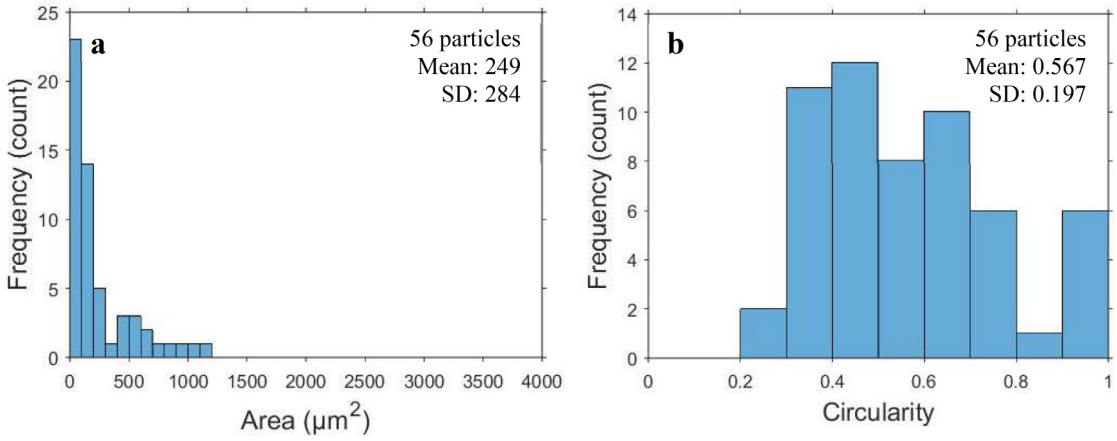

FIG. 7. Particle area (a) and circularity (b) histograms summarizing the size and shape of particle features in the secondary ion image of the mono-urea molecular ion [Fig. 6(b)].

the form of distinct particles within a continuous matrix, chemical analysis is needed for identification of the respective phases, which this technique is unable to confirm.

D. Chemical imaging and depth profiling with cryo-ToF-SIMS

SIMS can provide detailed insights into the spatial distribution of molecular species of interest in a sample. The main challenge associated with SIMS analysis of lubricating grease is the sample preparation. Namely, the volatile nature of the base oil components of the grease is incompatible with the ultrahigh vacuum present in the analysis chamber of a SIMS instrument, with their *in situ* removal at ambient temperatures presenting two issues: (i) loss of native-state structure and (ii) potential risk of instrument contamination. Hence, cryogenic sample preparation was necessary, which is inherently more challenging than the ambient sample preparation utilized for optical microscopy and CRM. The full optimized sample preparation procedure is shown in Fig. S3 in the supplementary material and described in detail in *Procedure S1* of the supplementary material. In brief, immediately following plunge freezing, the samples are transferred either within liquid nitrogen or within the vacuum of the Leica VCT, which is subsequently coupled directly to a precooled OrbiSIMS airlock maintained under vacuum. Importantly, once frozen, the samples do not experience contact with atmospheric conditions and are held in their frozen state. This prevents any frost formation upon the sample and retains the native structure of the sample.[39] Obtaining a surface suitable for analysis involved smearing the grease around the sample holder to increase the amount of material available for analysis and thus the chance of locating a flat surface. A ToF-SIMS spectrum obtained on a chosen area of the frozen grease identifying the mono-urea and ester base oil known to be present in the grease formulation (Table S1 in the supplementary material) is shown in Fig. 6(a).

TABLE I. Summary of mean particle area across the characterization techniques used throughout this study detailed in the main text. Italicized values were obtained from repeat analysis, as described in the supplementary material, where Mag = Magnification.

Technique	Mag	Image size (μm)	No of particles sampled	Mean area and SD (μm²)	Reference
POM	10×	1650 × 1380	591	165 ± 278	Figure 2
		as above	*492*	*165 ± 206*	*Figure S7*
POM	20×	830 × 690	154	161 ± 163	Figure 2
		as above	*125*	*216 ± 283*	*Figure S7*
cryo-SIMS	N/A	500 × 500	56	249 ± 284	Figure 7(a)
POM	50×	340 × 280	12	183 ± 199	Figure 2
		as above	*21*	*157 ± 208*	*Figure S7*
CRM	100×	300 × 300	16	279 ± 382	Figure 4(a)
		100 × 100	*n/a*	*n/a*	*Figure S8*

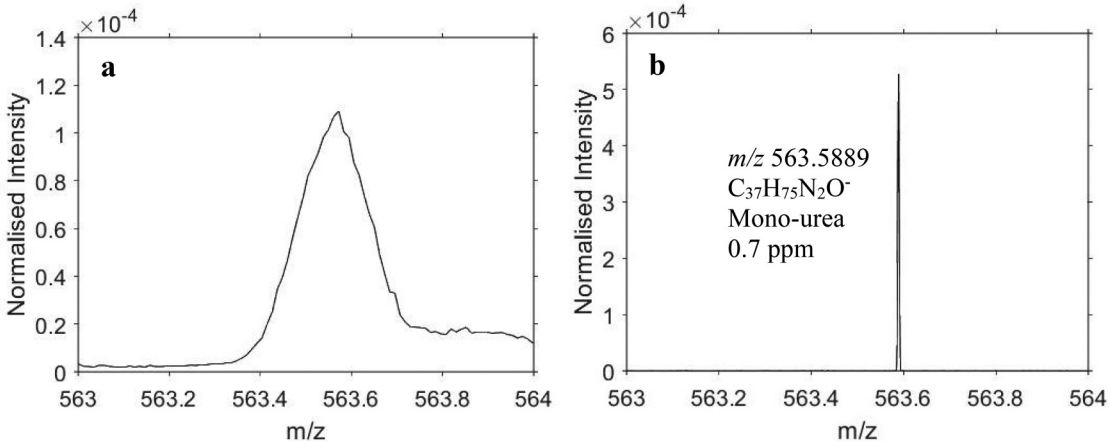

FIG. 8. Negative polarity (a) ToF-SIMS and (b) OrbiSIMS spectra collected from the plunge frozen commercial base polyurea grease, showing the 563–564 *m/z* mass range.

The distribution of the mono-urea molecular ion is in the form of particle-like structures. Ion images of the CN^- and CNO^- ions, likely fragments of the mono-urea, show a similar spatial distribution (Fig. S13 in the supplementary material). Ice clusters that have a different spatial distribution to the mono-urea ion image shown in Fig. 6(b) were also observed (Fig. S14 in the supplementary material). SIMS can also provide information on the distribution of molecular species of interest below the surface of a sample. This is important to (a) gain an understanding of the structure of a material in 3D and (b) confirm that the selected molecular species of interest are not surface contaminants. The 3D distribution of the mono-urea molecular ion is shown in Fig. 6(c). Here, it can be seen that particle-like structures exist in the z direction (below the surface), thereby confirming that the thickener phase exists in the form of distinct particles not just on the surface, but throughout the bulk of the material.

Particle area and circularity analyses were conducted on the structures identified in Fig. 6(b). The corresponding histograms are shown in Fig. 7.

Summaries of the mean particle area across all characterization techniques utilized in this study are shown in Table I.

In general, the mean area of the particle structures observed across all native state (POM and CRM) and near-native state techniques (cryo-SIMS) are comparable and within acceptable limits of each other. The variation is attributed to the number of particles sampled using each technique—at higher magnification (and smaller image sizes) fewer particles are inherently visible within the analyzed area. Indeed, the repeat CRM analysis shown in Fig. S8 in the supplementary material displays only two or three particle-like structures, all of which extend beyond the limits of the imaged area and thus extraction of size is not possible.

E. Confirmation of peak assignments with OrbiSIMS

To further confirm the mono-urea peak assignment, OrbiSIMS analysis was also conducted on the plunge frozen commercial grease formulation. Using an argon GCIB as the primary ion beam allows for the detection of intact ions. Additionally, utilizing an Orbitrap analyzer that exhibits superior mass resolving power to the ToF (>240 000 at *m/z* 200 vs > 30 000)[53] can allow for greater confidence when assigning peaks. The mono-urea peak in both ToF-SIMS and OrbiSIMS analyses of the commercial grease formulation is shown in Fig. 8. The full OrbiSIMS spectrum, showing the locations of the mono-urea and di-urea present in the commercial grease formulation, is shown in Fig. S15 in the supplementary material. The corresponding peak assignment for Fig. S15 in the supplementary material is shown in Table S2 in the supplementary material.

When examining the OrbiSIMS spectrum of the grease in the mass range where the mono-urea molecular ion peak is expected to be present, a single peak is visible [Fig. 8(b)]. Furthermore, the assignment of this peak as the expected mono-urea compound is within the acceptable deviation for OrbiSIMS analysis (<1 ppm). In addition, the mono-urea peak shown in Fig. 8(a) does not appear in ToF-SIMS analysis of the pure base oil components (Fig. S16 in the supplementary material), helping to further verify that the peak assigned as the mono-urea [Fig. 8(a)] is characteristic of the polyurea thickener component of the commercial grease formulation.

IV. SUMMARY AND CONCLUSIONS

In this study, we have successfully used two complementary chemical imaging techniques, namely, CRM and cryo-SIMS, to understand the structure of a commercial polyurea grease sample in its native and near-native state. Of particular significance is that it was possible to use SIMS to analyze lubricating grease and extract meaningful data, as grease type materials are considered incompatible with the high vacuum of an SIMS instrument. We have demonstrated that it is possible to freeze lubricating grease so that it is amenable to analysis via SIMS.

Both CRM and cryo-SIMS suggested that the polyurea thickener in this commercial grease formulation exists in the form of

distinct particles, which agreed with the POM and cryo-SEM analyses. Two main insights can be drawn from this. First, an understanding as to what "thickens" the base oil phase of this commercial grease system to give a high viscosity material. Using our novel combination of chemical analysis imaging techniques alongside optical microscopy, it is now understood with greater confidence that the thickener phase in this sample self-assembles to form particle-like structures. Second, POM, the most straightforward and fastest to utilize native-state technique, can be used with more confidence in isolation to understand the structure of future lubricants and compare their structure-performance relationship to existing commercial systems.

Future directions of the work demonstrated in this study include developing cross-platform correlative workflows for both ambient and cryogenic techniques. This was attempted for the purposes of this investigation; however, attempts were unsuccessful. Despite exhaustive experimentation, we concluded it was not possible to image the same area analyzed by CRM using POM due to the grease shifting when transferring between instruments. Likewise, correlative cryogenic analysis, i.e., transferring the same sample from cryo-SIMS to cryo-SEM, was also unsuccessful; this was attributed to the inherent challenges that occur with cryogenic sample preparation. We anticipate that imaging grease samples using a confocal Raman microscope equipped with an optical polarizer will solve the issue of sample mobility when transferring between ambient analytical platforms and will explore this in our future work. Similarly, we will continue to develop cryogenic sample preparation and cross-platform transfer protocols, as this represents an important and timely challenge, applicable to a plethora of complex sample types, from foodstuffs and textiles to healthcare products and cosmetics.

SUPPLEMENTARY MATERIAL

See the supplementary material for detailed definitions of the characterisation and methodologies that were used to support the analysis of the commercial base polyurea grease. It includes a definition of the reagent composition of the commercial grease supplied by the external collaborator, diagrams outlining both the industrial manufacturing process and the reaction pathways leading to different urea products that result from application of this process. The experimental protocol used for Cryo 3D OrbiSIMS analysis is also described in full, together with a workflow for cryogenic sample preparation. Additional, transmission brightfield optical microscopy images of polyurea particles extracted from the grease acquired at multiple magnifications are included, along with the associated particle-size and circularity distributions. Chemical imaging through confocal Raman microscopy is presented, together with cryo-SEM analysis and ToF-SIMS ion images highlighting key anionic species, ice-related features and the mono-urea and di-urea molecular moieties which is supported by a summary of the assigned molecular ions.

ACKNOWLEDGMENT

We would like to thank the Engineering and Physical Sciences Research Council (No. EP/V51973X/1) for funding of the research.

AUTHOR DECLARATIONS

Conflict of Interest

The authors have no conflicts to disclose.

Author Contributions

Xiao Yuan L. Wang: Data curation (equal); Formal analysis (equal); Investigation (equal); Methodology (equal); Writing – original draft (equal). **Christopher D. J. Parmenter:** Data curation (equal); Formal analysis (equal); Investigation (equal); Methodology (equal); Writing – review & editing (equal). **Anna M. Kotowska:** Data curation (equal); Formal analysis (equal); Investigation (equal); Methodology (equal); Writing – review & editing (equal). **Julie A. Watts:** Data curation (equal); Formal analysis (equal); Investigation (equal); Methodology (equal); Writing – review & editing (equal). **Davide S. A. De Focatiis:** Data curation (equal); Formal analysis (equal); Investigation (equal); Methodology (equal); Supervision (equal); Writing – review & editing (equal). **Graham A. Rance:** Data curation (equal); Formal analysis (equal); Investigation (equal); Methodology (equal); Supervision (equal); Writing – review & editing (equal). **David J. Scurr:** Conceptualization (equal); Data curation (equal); Formal analysis (equal); Investigation (equal); Methodology (equal); Supervision (equal); Writing – review & editing (equal). **Derek J. Irvine:** Conceptualization (equal); Funding acquisition (equal); Investigation (equal); Methodology (equal); Project administration (equal); Resources (equal); Supervision (equal); Writing – review & editing (equal).

DATA AVAILABILITY

The data that support the findings of this study are available from the corresponding authors upon reasonable request.

Nomenclature

CRM	Confocal Raman microscopy
Cryo-SEM	Cryogenic scanning electron microscopy
Cryo-SIMS	Cryogenic secondary ion mass spectrometry
EDX	Energy dispersive X-ray
GCIB	Gas cluster ion beam
LMIG	Liquid metal ion gun
MCR	Multivariate curve resolution
POM	Polarized optical microscopy
SD	Standard deviation
SEM	Scanning electron microscopy
SIMS	Secondary ion mass spectrometry
TEM	Transmission electron microscopy
ToF-SIMS	Time-of-flight secondary ion mass spectrometry

REFERENCES

[1]P. S. Venkataramani, R. G. Srivastava, and S. K. Gupta, J. Synth. Lubr. **4**, 229 (1987).
[2]A. S. Lyadov, Y. M. Maksimova, A. S. Shakhmatova, V. V. Kirillov, and O. P. Parenago, Russ. J. Appl. Chem. **91**, 885 (2018).
[3]B. P. Tonkonogov, A. Y. Kilyakova, N. D. Stenina, O. V. Popova, R. Z. Safieva, V. A. Vinokurov, S. N. Gorbacheva, and S. O. Il'in, Chem. Technol. Fuels Oils **55**, 689 (2020).

[4]G. Ren, X. Sun, W. Li, H. Li, L. Zhang, X. Fan, D. Li, and M. Zhu, Friction **9**, 1077 (2021).
[5]G. Calderon-Salmeron, J. Leckner, R. Westbroek, B. Chanamolu, and S. Glavatskih, Tribol. Int. **198**, 109777 (2024).
[6]C. J. Donahue, J. Chem. Educ. **83**, 862 (2006).
[7]X. Fan, W. Li, H. Li, M. Zhu, Y. Xia, and J. Wang, Tribol. Int. **118**, 128 (2018).
[8]K. Hanabusa and M. Suzuki, Polym. J. **46**, 776 (2014).
[9]D. K. Smith, Soft Matter **20**, 10 (2024).
[10]L. Li, R. Zheng, and R. Sun, J. Adv. Res. **69**, 91 (2025).
[11]P. Ding, W. Cao, Q. Ding, C. Liu, W. Yu, and L. Hu, J. Mater. Res. Technol. **35**, 7074 (2025).
[12]J. Wang, Z. Guo, W. Hu, H. Lu, and J. Li, Tribol. Int. **194**, 109573 (2024).
[13]M. A. Delgado, M. C. Sánchez, C. Valencia, J. M. Franco, and C. Gallegos, Chem. Eng. Res. Des. **83**, 1085 (2005).
[14]C. Roman, C. Valencia, and J. M. Franco, Tribol. Lett. **63**, 20 (2016).
[15]D. Muller, C. Matta, R. Thijssen, M. N. Bin Yusof, M. C. P. Van Eijk, and S. Chatra, Tribol. Int. **110**, 278 (2017).
[16]M. A. Thorseth, J. D. Harris, J. Gu, J. Cuthbert, L. Huffman, K. Capaldo, and Z. Jia, Microsc. Microanal. **27**, 12 (2021).
[17]F. Cyriac, P. M. Lugt, R. Bosman, C. J. Padberg, and C. H. Venner, Tribol. Lett. **61**, 18 (2016).
[18]G. Ren, C. Zhou, X. Fan, M. Zheng, and S. Wang, Tribol. Int. **173**, 107643 (2022).
[19]P. M. Lugt, Tribol. Trans. **52**, 470 (2009).
[20]L. Ahme, E. Kuhn, and M. Á. Delgado Canto, Tribol. Int. **187**, 108771 (2023).
[21]J. Wang, Z. Guo, W. Hu, X. Li, H. Lu, and J. Li, Macromolecules **57**, 5486 (2024).
[22]H. Wu, J. Wang, Z. Guo, H. Du, W. Hu, J. Xu, J. Wang, H. Lu, and J. Li, Tribol. Int. **204**, 110526 (2025).
[23]L. Salomonsson, G. Stang, and B. Zhmud, Tribol. Trans. **50**, 302 (2007).
[24]T. Lombardo, F. Walther, C. Kern, Y. Moryson, T. Weintraut, A. Henss, and M. Rohnke, J. Vac. Sci. Technol. A **41**, 053207 (2023).
[25]Y. Ilin and M. L. Kraft, Curr. Opin. Biotechnol. **31**, 108 (2015).
[26]E. S. Allakhverdiev, B. D. Kossalbayev, A. K. Sadvakasova, M. O. Bauenova, A. M. Belkozhayev, O. V. Rodnenkov, T. V. Martynyuk, G. V. Maksimov, and S. I. Allakhverdiev, J. Photochem. Photobiol., B **252**, 112870 (2024).
[27]T. Touzalin, S. Joiret, I. T. Lucas, and E. Maisonhaute, Electrochem. Commun. **108**, 106557 (2019).
[28]R. Kozdrach, Processes **12**, 565 (2024).
[29]D. N. Khaemba, A. Neville, and A. Morina, RSC Adv. **6**, 38637 (2016).
[30]C. E. Garcia, M. Ueda, H. Spikes, and J. S. S. Wong, Sci. Rep. **11**, 3621 (2021).
[31]A. Priebe and J. Michler, Materials **16**, 2090 (2023).
[32]I. S. Gilmore, S. Heiles, and C. L. Pieterse, Annu. Rev. Anal. Chem. **12**, 201 (2019).
[33]Z. Shen and S. Fearn, J. Electroceram. **53**, 103 (2025).
[34]P. Agüi-Gonzalez, S. Jähne, and N. T. N. Phan, J. Anal. At. Spectrom. **34**, 1355 (2019).
[35]M. K. Passarelli *et al.*, Nat. Methods **14**, 1175 (2017).
[36]S. J. Lee, C. M. Choi, B. K. Min, J. Y. Baek, J. Y. Eo, and M. C. Choi, Bull. Korean Chem. Soc. **40**, 877 (2019).
[37]S. Ninomiya, Y. Nakata, K. Ichiki, T. Seki, T. Aoki, and J. Matsuo, Nucl. Instrum. Methods Phys. Res., Sect. B **256**, 493 (2007).
[38]I. Yamada, J. Matsuo, N. Toyoda, and A. Kirkpatrick, Mater. Sci. Eng., R **34**, 231 (2001).
[39]J. Zhang *et al.*, Anal. Chem. **92**, 9008 (2020).
[40]C. Kern, A. Scherer, L. Gambs, M. Yuneva, H. Walczak, G. Liccardi, J. Saggau, P. Kreuzaler, and M. Rohnke, Chem.: Methods **4**, e202400008 (2024).
[41]M. Taylor, D. Scurr, M. Lutolf, L. Buttery, M. Zelzer, and M. Alexander, Biointerphases **11**, 02A301 (2016).
[42]C. L. Newell, J. L. Vorng, J. I. MacRae, I. S. Gilmore, and A. P. Gould, Angew. Chem., Int. Ed. **59**, 18194 (2020).
[43]N. J. Starr *et al.*, Proc. Natl. Acad. Sci. U.S.A **119**, e2114380119 (2022).
[44]A. Akbari, A. Galstyan, R. E. Peterson, H. F. Arlinghaus, and B. J. Tyler, Anal. Bioanal. Chem. **415**, 991 (2023).
[45]Q. Zhao, E. Zhang, W. Li, W. Lou, J. Dong, X. Wang, and R. Zhang, Tribol. Int. **193**, 109458 (2024).
[46]Y. Yoshida, Y. Furushima, T. Yamamoto, and B. Mizaikoff, Polym. Compos. **45**, 7427 (2024).
[47]A. K. Kuptsov, E. V. Zhmaeva, A. V. Kulik, and K. B. Rudyak, Chem. Technol. Fuels Oils **58**, 772 (2022).
[48]Y. Mido, F. Fujita, H. Matsuura, and K. Machida, Spectrochim. Acta, Part A **25**, 16 (2010).
[49]F. Adar, Spectroscopy **25**, 16 (2010), see https://www.spectroscopyonline.com/view/transmission-raman-method-quantifying-bulk-materials#:~:text=The%20main%20goal%20of%20a,1%20s%20to%200.1%20s.
[50]C. Efthymiou, M. A. K. Williams, and K. M. McGrath, Food Hydrocolloids **73**, 203 (2017).
[51]I. Davidovich, C. Levin, and Y. Talmon, J. Microsc. **299**, 132 (2025).
[52]V. Massardier, L. Voron, C. Esnouf, and J. Merlin, J. Mater. Sci. **36**, 1363 (2001).
[53]C. Kern, S. Kern, A. Henss, and M. Rohnke, Biointerphases **18**, 041203 (2023).